Published in final edited form as:
Clin Exp Metastasis. 2013 March ; 30(3): . doi:10.1007/s10585-012-9531-z.

Cytoskeletal stiffness, friction, and fluidity of cancer cell lines with different metastatic potential

Mark F. Coughlin,
Molecular and Integrative Physiological Sciences, Department of Environmental Health, Harvard School of Public Health, 665 Huntington Avenue, Boston, MA 02115, USA

Diane R. Bielenberg,
Vascular Biology Program, Boston Children's Hospital, Department of Surgery, Harvard Medical School, 300 Longwood Avenue, Boston, MA 02115, USA

Guillaume Lenormand,
Molecular and Integrative Physiological Sciences, Department of Environmental Health, Harvard School of Public Health, 665 Huntington Avenue, Boston, MA 02115, USA

Marina Marinkovic,
Molecular and Integrative Physiological Sciences, Department of Environmental Health, Harvard School of Public Health, 665 Huntington Avenue, Boston, MA 02115, USA

Carol G. Waghorne,
ArQule, 19 Presidental Way, Woburn, MA 01801, USA

Bruce R. Zetter, and
Vascular Biology Program, Boston Children's Hospital, Department of Surgery, Harvard Medical School, 300 Longwood Avenue, Boston, MA 02115, USA

Jeffrey J. Fredberg
Molecular and Integrative Physiological Sciences, Department of Environmental Health, Harvard School of Public Health, 665 Huntington Avenue, Boston, MA 02115, USA

Abstract

We quantified mechanical properties of cancer cells differing in metastatic potential. These cells included normal and H-ras-transformed NIH3T3 fibroblast cells, normal and oncoprotein-overexpressing MCF10A breast cancer cells, and weakly and strongly metastatic cancer cell line pairs originating from human cancers of the skin (A375P and A375SM cells), kidney (SN12C and SN12PM6 cells), prostate (PC3M and PC3MLN4 cells), and bladder (253J and 253JB5 cells). Using magnetic twisting cytometry, cytoskeletal stiffness (g') and internal friction (g'') were measured over a wide frequency range. The dependencies of g' and g'' upon frequency were used to determine the power law exponent x which is a direct measure of cytoskeletal fluidity and quantifies where the cytoskeleton resides along the spectrum of solid-like ($x = 1$) to fluid-like ($x = 2$) states. Cytoskeletal fluidity x increased following transformation by H-ras oncogene expression in NIH3T3 cells, overexpression of ErbB2 and 14-3-3-ζ in MCF10A cells, and implantation and growth of PC3M and 253J cells in the prostate and bladder, respectively. Each of these perturbations that had previously been shown to enhance cancer cell motility and invasion are shown here to shift the cytoskeleton towards a more fluid-like state. In contrast, strongly metastatic A375SM and SN12PM6 cells that disseminate by lodging in the micro-circulation of

mark_coughlin@verizon.net.

Conflict of interest The authors declare that they have no conflict of interest.

peripheral organs had smaller *x* than did their weakly metastatic cell line pairs A375P and SN12C, respectively. Thus, enhanced hematological dissemination was associated with decreased *x* and a shift towards a more solid-like cytoskeleton. Taken together, these results are consistent with the notion that adaptations known to enhance metastatic ability in cancer cell lines define a spectrum of fluid-like versus solid-like states, and the position of the cancer cell within this spectrum may be a determinant of cancer progression.

Keywords

Cytoskeletal fluidity; Dynamic modulus; Magnetic twisting cytometry; Metastasis; Metastatic potential

Introduction

The principal cause of pain, suffering, and death in most cancers is the metastatic lesion [1]. Despite an enormous public health burden attributed to metastatic disease, the primary determinants of metastasis remain poorly understood. Layers of homeostatic barriers prevent metastatic dissemination of primary tumor cells, thereby making the metastatic process largely inefficient [cf. 2, 3]. Within the proliferating primary tumor population there arise genetic mutations, chromosomal rearrangements, and epigenetic alterations [3] affecting nearly every facet of cancer cell biology [3, 4]. Detailed genetic and proteomic analyses reveal specific adaptations that seem to endow the primary tumor cell with the aggressive traits enabling metastasis [cf. 5, 6]. Interestingly, these adaptations exhibit extensive cancer-specific and cell-specific diversity. By contrast, the underlying physical processes mediating dissemination from most solid tumors seem to be remarkably similar, suggesting, superficially at least, that metastatic dissemination in diverse cancers may be enabled through common biophysical adaptations. To date, however, the biophysical basis of metastatic ability remains poorly understood.

Advancing through the metastatic process is accompanied by biophysical adaptations in cancer cells. Escape from the primary tumor and invasion into the surrounding tissue requires detachment from physical constraints of the underlying matrix and neighboring cells. Strongly metastatic cells typically express fewer adhesion receptors and exhibit increased protease activity facilitating their separation from their environment [7–11]. This loss of substrate contact leads not only to strongly metastatic cells exhibiting rounded cell morphologies [12] but also loss of cytoskeletal tension [13]; in normal cells, cytoskeletal tension is a key determinant of nearly every facet of cytoskeletal biophysics including stability [14], stiffness [15], internal friction [15], remodeling [16], traction [17], and fluidity [15, 18]. Weakly and strongly metastatic cells exhibit different motile strategies [19–21]. A program of systematic dedifferentiation leads metastatic cells to shift their motile strategy from the polarized, mesenchymal-like motility associated with highly rigid, strongly contractile cells (e.g., fibroblasts) to the non-polarized, amoeboid-like motility associated with highly deformable, weakly contractile cells (e.g., leukocytes). Although motile control is multifaceted, the Rho-family of small GTPases plays a key role in determining motile strategy through regulation of cyto-skeletal architecture and dynamics [22, 23]. This shift in cytoskeletal organization allows strongly metastatic cells to penetrate the dense extracellular matrix surrounding blood vessels that presents a barrier to less invasive tumor cells. Cancer cells are notably more fragile than non-cancerous cells [24, 25], and cancer cell destruction by hematological forces is an important and potent anti-metastatic mechanism [24, 26–28]. Strongly metastatic cells are better able than weakly metastatic cells to survive intravasation [19, 21] through a mechanism that may involve cytoskeletal reorganization and reinforcement through intermediate filament synthesis [29].

Taken together, these observations suggest that cancer progression might be coupled to changes in cytoskeletal mechanics. To explore this possibility, we used magnetic twisting cytometry with optical detection (OMTC) [15] to assess cytoskeletal stiffness, internal friction, and fluidity over four decades of oscillatory frequency (0.1–1,000 Hz) applied to cancer cell lines that differ in metastatic potential. Our principal finding is that within this frequency range, cytoskeletal fluidity, but not cytoskeletal stiffness or friction, is correlated with cancer progression.

Materials and methods

Cell lines

NIH3T3 cells are mouse embryo fibroblasts that are nontumorigenic and non-metastatic. Transfection of NIH3T3 cells with a plasmid vector pcDNA3 containing the H-ras-oncogene (Invitrogen) renders the cells tumorigenic and metastatic in mice [30]. NIH3T3 cells were obtained from ATTC (CRL-1658).

MCF10A cells are a human mammary epithelial cell line that is non-metastatic [31]. Sublines MCF10A-ErbB2, MCF10A-ζ, and MCF10A-ErbB2-ζ overexpress the onco-proteins ErbB2, 14-3-3-ζ, and both, respectively, with MCF10A-V cells transfected with vector serve as control [32]. Overexpression of either ErbB2 or 14-3-3-ζ alone in cultured cells imparts some characteristics of transformation [33, 34] and overexpression of 14-3-3-ζ in mouse mammary tumor cells leads to a higher incidence of pulmonary metastases [33]. Co-overexpression of both ErbB2 and 14-3-3-ζ drives the transition from localized ductal carcinoma in situ to invasive breast cancer [33]. Transfected MCF10A cells were kindly provided by Dr. Muhammad Zaman (Boston University, Boston, MA).

253J cells are a human bladder epithelial cell line [35] that is weakly tumorigenic and are expected to be at best very weakly metastatic, although metastatic ability of 253J cells was not determined [36]. 253JB5 cells are a sub-population of 253J cells that are strongly tumorigenic and strongly metastatic [36]. PC3M cells are a human prostate tumor cell line that is highly tumorigenic and metastatic [37]. PC3MLN4 cells are a subpopulation of PC3M cells that exhibit similar tumorigenic and metastatic characteristics as PC3M cells, however with the PC3MLN4 variant exhibiting a slightly higher incidence of distant metastases [37]. A375P cells are a human melanoma cell line that is highly tumorigenic but weakly metastatic [38, 39]. A375SM cells are a subpopulation of A375P cells that are strongly tumorigenic and metastatic [38, 39]. SN12C cells are a primary human renal tumor cell line [40] that is highly tumorigenic but weakly metastatic [41]. SN12PM6 cells are a highly metastatic subpopulation of SN12C cells that produce lesions in the lung, liver, pancreas, seminal vesicles, lymph nodes and ascites [41]. The strongly and weakly metastatic cancer cell line pairs were kindly provided by Dr. Isaiah J. Fidler (M.D. Anderson Cancer Center).

Cell culture

Normal and RAS-transformed NIH3T3 fibroblast cells were maintained in MEM with 10 % bovine calf serum. PC3M and PC3MLN4 cells were maintained in RPMI (Gibco) supplemented with 10 % FBS, 1 mM Sodium pyruvate, 1 % non-essential amino acids (Gibco), 1 % vitamin solution (Gibco), 1 % penicillin–streptomycin-glut (Sigma). MCF-10A cells maintained in DMEM/F12 with 5 % horse serum, 20 ng/ml epidermal growth factor, 0.5 μg/ml hydrocortisone, 100 ng/ml cholera toxin, 10 μg/ml insulin, and 1 % penicillin–streptomycin (Sigma). Fibroblasts and MCF-10A cells were plated in plastic culture flasks and maintained in humidified atmosphere at 37 °C and 5 % CO_2. All other cell lines were maintained in MEM with 10 % FBS, 1 mM sodium pyruvate, 1 % non-essential amino

acids, 1 % vitamin solution, 1 % penicillin–streptomycin and 2 mM L-glutamine on plastic culture flasks in a humidified atmosphere at 37 °C and 10 % CO_2.

Cells were trypsinized (0.25 % trypsin; Sigma) and plated at 20,000 cells per uncoated glass bottom well (MatTek, Ashland, MA) except 253JB5 cells which were plated up to 40,000 cells per well. After 24–48 h, cells were typically well-spread and either grew to confluence or as islands of neighboring cells. 253JB5 cells tended to grow as well-dispersed isolated cells and plating at higher densities produced more observations per well. Cancer cell biophysics was then assessed.

Magnetic twisting cytometry with optical detection (OMTC)

Solid Fe_3O_4 ferrimagnetic beads (diameter = 4.5 μm) produced in our laboratory were coated with a synthetic peptide containing the sequence RGD (Peptite 2000; Integra LifeSciences, San Diego, CA) at 50–150 μg of ligand per milligram of beads by overnight incubation at 4 °C in carbonate buffer (pH 9.4). Cells were prepared for experiments by washing twice with media, and incubated with RGD-coated beads for 10 min at 37 °C to allow binding specifically to integrin receptors on the cell surface. The wells were washed twice with media to remove unbound beads. The final concentration of beads was approximately one per cell.

Glass-bottom wells containing cells with attached beads were observed on the stage of an inverted microscope (Leica Model #DM IRBE, Leica Microsystems, Wetzlar, Germany) and viewed under bright-field with 20× objective (NA 0.4) or 10× for MCF10A cell lines. Beads were magnetized in the horizontal plane of the culture plate converting each bead into a permanent magnet. A small oscillating magnetic field applied in the vertical plane induced a mechanical torque which caused each bead to rotate towards alignment like a compass needle in a magnetic field. Attached beads underwent a measurable lateral displacement in addition to a small rotation. Bead motion was tracked through images captured by CCD camera (Model #JAI CV-M10, JAI PULNiX, San Jose, CA) with exposure time of 0.1 ms and acquisition frequency of 12 Hz. From recorded images, the bead position was computed using an intensity-weighted center-of-mass algorithm yielding spatial resolution greater than 5 nm [42]. Measurements were performed at oscillatory frequencies between 0.1 and 1,000 Hz with heterodyning employed at twisting frequencies above 1.5 Hz.

Biophysical characterization

Oscillatory twisting of cell-bound beads enabled measurement of both cytoskeletal stiffness g' and friction g'' on a bead-by-bead basis. The imposed oscillatory magnetic field induced in each bead a torque $T(t) = c \cdot H(t) \cdot \cos[\theta(t)]$, where $H(t)$ is the strength of the magnetic field in units of Gauss, c is the bead constant in units of torque per unit bead volume per Gauss, and $\theta(t)$ is the angle of the bead's magnetic moment relative to the original magnetization direction [43–45]. The bead constant c relates the strength of the magnetic field to the induced bead torque and is determined by independent calibration by measuring the angular velocity of beads twisted in a fluid of known viscosity [46]. The term $\cos[\theta(t)]$ was taken as unity in computing bead torque. For the small lateral bead displacements used in this study $d(t)$ (<100 nm) and assuming beads rotate about a fixed pivot at the cell surface, $\theta(t)$ was small (<0.05°) and contributed a very small error to $T(t)$ ($\ll$1 %). The induced torque in each bead has units of stress, Pa. From the ratio of lateral bead displacement to twisting field $T(t)$, g' and g'' are computed by Fourier transformation according to [44]

$$g' + ig'' = \bar{T}(t) / \bar{d}(t) \quad (1)$$

where $i^2 = -1$ is the imaginary unit and overbar indicates Fourier transformation. Stiffness g' and friction g'' as defined in Eq. (1) have units of Pa/nm.

Only individual beads attached to the apical surface of a cell were selected for analysis. Some beads were eliminated from further analysis based on their motion [44]. Beads whose amplitude of lateral displacement d_0 was below the system noise level (20 nm), energy at higher harmonics exceeding 18 % of the fundamental amplitude, or movement in the magnetization direction exceeded the orthogonal direction were not analyzed. Beads were also discarded if they produced an unrealistic modulus measurement (e.g., a nonpositive g') even at a single frequency. Typically 60–75 % of the beads met these criteria and were analyzed, although the exact number depended on the cell type. These criteria insure we report the biophysical properties of cancer cells from the linear regime.

Measurements in a variety of cell types, with a wide panel of probe ligands, and with many blunt interventions have shown that g' and g'' increase with frequency following a weak power law before g'' was dominated by an additive Newtonian viscosity at high frequencies. These features of g' and g'' spectra conform to an empirical description known in the engineering literature as structural damping [15, 47, 48]:

$$\bar{g}' + i\bar{g}'' = A(i\omega)^{x-1}\Gamma(2-x) + i\omega\mu \quad (2)$$

where A is a scaling factor, $\omega = 2\pi f$ with f the twisting frequency, $\Gamma(\cdot)$ is the Gamma function, μ is an additive frictional term, and $x - 1$ is the power law exponent of ω. Equation (2) allows quantitative identification of the parameters A, μ, and x from measurements of g' and g'' [44, 49]. Taking $x = 1$ and $\omega = 0$ (i.e., the static case) shows that stiffness is a constant, $g' = A$, and friction is zero, $g'' = 0$, revealing the material to be an ideal elastic solid with stiffness A. As x approaches 2, stiffness goes to zero $g' = 0$ and friction becomes large revealing the material to be a purely viscous fluid. Values of x between 1 and 2 describe a material intermediate between an elastic solid (zero fluidity) and Newtonian fluid (ideal fluid). Thus, x describes material fluidity [15, 44, 48].

Least-squares minimization evaluated x on a bead by bead basis as described previously [44, 49]. Since g' and g'' followed log-normal distributions (see below), least-squares minimization was taken over the squared differences between the logarithm of g' and g'' data and the logarithm of Eq. (2). The methodological limitations and validation of OMTC have been discussed in detail elsewhere [44].

Comparing mean values

Distributions of d, and consequently, g' and g'' were truncated because beads whose motion falls below the level of system noise are ignored (Fig. 1). To accurately assess distribution mean μ and standard deviation σ, distributions were fitted with the normal distribution curve $n = \frac{1}{\sqrt{2\pi}\sigma} e^{-\frac{(d-\mu)^2}{2\sigma^2}}$, where n is the number of observations in a particular bin, d is the displacement of a particular bin, using a nonlinear least-squares method.

Normality was evaluated using two fundamentally different approaches, the simple Chi-square goodness-of-fit test and the preferred D'Agostino–Pearson K^2 test. Informal evaluation of normality is provided graphically by normal probability plots in which ordered data is displayed against the outcome that would be obtained from normally distributed data. Departures from normality become evident in data that deviate from linearity. Recognizing that small deviations from normality strongly influence normality tests but prove irrelevant in inferential statistics (e.g., t tests), mean values between cell lines were compared using two procedures. The common non-pooled t-procedure (t test) compares mean values of two

populations whose samples are normally distributed [50]. The two-sample *z*-procedure (*z* test) compares mean values of two populations whose samples are independent and large (sample size = 30), but not necessarily normal [50]. Both *z* and *t* tests were evaluated with two-tails at 5 % probability.

Results

RGD-coated beads bound avidly the cells (Fig. 2). Beads came into sharp focus above the apical cell surface indicating that the beads were on top of the cells. The degree of bead internalization following the 10 min incubation period was not measured. Applying an oscillating twisting field rocked the attached beads side to side. The magnitude of the twisting field was adjusted to produce mean bead displacement amplitudes near 100 nm at the low frequency $f = 0.1$ Hz (Fig. 3). Limiting the amplitude of the twisting field in this way minimized nonlinear mechanical responses [44, 51, Table 1]; beads exhibiting nonlinearities were rejected from analysis.

Cytoskeletal biophysics was characterized by varying the frequency of the oscillatory twisting field and using the induced bead motion to compute cytoskeletal stiffness g' and friction g''. Normal and RAS-transformed NIH3T3 cells, MCF10A-V, MCF10A-ErbB2, MCF10A-ζ, and MCF10A-ErbB2-ζ cells, 253J and 253JB5 cells, PC3M and PC3MLN4 cells, A375P and A375SM cells, and SN12C and SN12PM6 cells exhibited qualitatively similar g' and g'' spectra (Fig. 4). Stiffness g' of all cell lines increased as a weak power law of frequency *f* and exponent *x* as seen by a nearly linear dependence of g' on *f* on log–log scales. Quantifying linearity using the linear correlation coefficient (R^2) of the least squares fit to the log g' versus log *f* data showed all cells were close to one with values falling in the range 0.9701 (MCF10A-V) to 0.9993 (SN12C). Friction g'' spectra within each cell line group were remarkably similar, however, there were qualitative differences between cell groups. Friction g'' of all MCF10A cell lines increased with the same weak power law dependence on *f* as stiffness g' (Fig. 4b). This indicates that little energy dissipation in MCF10A cell lines is attributed to purely viscous mechanisms between 0.1 and 1,000 Hz. At low *f*, g'' of 3T3, 3T3RAS, 253J, 253JB5 and SN12C cells was nearly constant or increased slightly before increasing rapidly above ~100 Hz (Fig. 4a, c, f). This strong *f* dependence of g'' above 100 Hz is consistent with viscous dissipation. In the remaining cell lines, g'' initially decreased slightly with increasing *f* before exhibiting the same strong *f* dependence at higher *f* (Fig. 4d, e, f). A negative *f* dependence in g'' with positive *f* dependence in g' is unexpected within the structural damping hypothesis, (Eq. 2). Instead, this low frequency behavior is seen in materials undergoing physical aging where material properties are slowly evolving over time [47, 52]. While evidence of physical aging has been reported in living cells [16, 53], its appearance in g'' spectra in these cancer cell lines is new and requires further investigation. Overall, g' and g'' spectra were well described by structural damping on a bead-by-bead basis. Thus, structural damping behavior was observed in both normal cells and tumor cell lines and was preserved following RAS-transformation, oncoprotein overexpression, acquisition of tumorigenicity, acquisition of invasive traits, and acquisition of metastatic ability. Quantitatively, g' and g'' spectra of cancer cells were similar to previous OMTC measurements on mouse embryo carcinoma cells [15] and human melanoma cell lines [53].

To determine if cytoskeletal deformability varied with metastatic potential, g' was compared between cells within each group. Since g' at each *f* was widely distributed in a log-normal fashion, the logarithm of the data followed a truncated normal distribution (Fig. 5a). Wide distributions of physical properties, sometimes reaching several orders of magnitude, characterize living cells probed by OMTC [42, 44] and other techniques [54–57]. Measuring from a large number of beads (Table 1) allowed these wide distributions to be well-defined

thereby giving highly confi-dent estimates of the geometric mean values and standard deviations. Mean g' at the low frequency $f = 0.1$ Hz from all cell lines fell in a narrow range confined within a single order of magnitude (Fig. 5b). Cells within each group were characterized by g' measurements that were quantitatively similar (Fig. 5b). The largest difference in g' between cells within a single group was between MCF10A-V and MCF10A-ζ cells, the latter of which was half of the former. However, differences in g' across groups reached nearly a factor of three between the NIH3T3, MCF10A, and PC3M groups and the A375P, SN12C, and 253J groups (Fig. 5b). Stiffness of NIH3T3 fibroblasts increased with H-ras-transformation as did MCF10A cells following full transformation by co-overexpression of ErbB2 and 14-3-3-ζ [33]. Similarly, g' of A375P cells increased with enhanced metastatic ability in A375SM cells (Fig. 5b). No difference in g' was detected between strongly metastatic 253JB5 and PC3MLN4 cells and their weakly metastatic counterparts, 253J and PC3M, respectively. Finally, g' of SN12C cells decreased with enhanced metastatic ability in SN12PM6 cells (Fig. 5b). Thus, in the cell lines tested here acquisition of tumorigenicity or enhanced metastatic ability did not induce large or systematic changes in cytoskeletal stiffness.

To determine if cytoskeletal friction varied with metastatic potential, g'' was compared between cells within each group. Like g', g'' was also widely distributed in a log-normal fashion, so the logarithm of the data appeared normally distributed (Fig. 6a). Mean friction at the low frequency $f = 0.1$ Hz spanned a range spanning an order of magnitude. Within cell groups, g'' increased (MCF10A-V and 253J cells), decreased (NIH3T3 and SN12C cells), or did not change (A375P and PC3M cells) following transformation or enhanced metastatic ability (Fig. 6b). Thus, the changes in cytoskeletal friction g'' between cell lines with different metastatic potential were neither large nor systematic.

Stiffness g' and friction g'' spectra were used to compute cytoskeletal fluidity x on a bead-by-bead basis. Despite strong qualitative consistency between x distributions and the normal curve (Fig. 7a), both the Chi-square goodness-of-fit test and the D'Agostino–Pearson K^2 test did not support the hypothesis of normality at 5 % significance. Normal probability plots deviated from linearity at high x indicating heavier right tails than would be expected for a normal distribution (Fig. 7b). Mean values of x from all cell lines fell with the narrow range $1.10 < x < 1.23$ which is quantitatively similar to non-cancerous cells under a wide variety of conditions $1.1 < x < 1.3$ [15, 16, 18, 44, 49]. Mean values of x were quantitatively similar within each group with the exception of MCF10A-ζ cells which spanned much higher x values than MCF10A-V, MCF10A-ErbB2, and MCF10A-ErbB2-ζ cells (Fig. 7c). H-ras-transformed NIH3T3 cells had a higher x than normal NIH3T3 cells. This indicates that transformation by the H-ras oncogene shifts the cytoskeleton towards a more fluid-like state. Similarly, MCF10A-ErbB2 and MCF10A-ζ cells had higher x than control MCF10A-V cells. Thus, overexpression of oncoproteins ErbB2 or 14-3-3-ζ, which individually imparts some characteristics of transformation upon MCF10A cells, also shifted the cytoskeleton towards a more fluid-like state. Co-overexpression of both ErbB2 and 14-3-3-ζ were not additive in x as MCF10A-ErbB2-ζ cells had higher x than MCF10A-ErbB2 cells but not MCF10A-ζ cells. Thus, co-overexpression of ErbB2 and 14-3-3-ζ oncoproteins, which is known to drive the invasive phenotype in breast cancer cells [33] shifted the cytoskeleton towards a more fluid-like state than the control cells. The strongly metastatic bladder cancer cell line 253JB5 had higher x than the weakly metastatic 253J cells (Fig. 7c). Similarly, the metastatic prostate cancer cell line PC3MLN4 had higher x than PC3M cells (Fig. 7c). Thus, the adaptations that increase metastatic ability in 253J and PC3M cells also shifted the cytoskeleton towards more fluid-like states. In contrast, x of the strongly metastatic melanoma cell line A375SM and kidney cancer cell line SN12PM6 were lower than their weakly metastatic counterparts A375P and SN12C, respectively (Fig. 7c). Thus, the

adaptations in A375P and SN12C cells that enable pulmonary colonization also shift the cytoskeleton towards more solid-like states.

Discussion

Our central hypothesis is that metastasis from solid tumors is enabled by biophysical alterations in cancer cells. As a preliminary step towards testing this hypothesis, we determined if cancer cell lines known to differ in metastatic ability exhibited alterations in cytoskeletal stiffness, friction, or fluidity. Directly assessing the biophysical properties of primary human cell line pairs revealed cytoskeletal fluidity as a potentially important correlate of cancer progression. The human bladder tumor cell line 253J was adapted to culture from a lymph node metastasis of a patient with multiple transitional cell cancers of the urinary tract [35]. In the nude mouse, 253J cells are weakly tumorigenic and likely to be only weakly metastatic [36]. Repeated cycles of implantation and growth of 253J cells in the bladder wall produced the highly metastatic 253JB5 cells [36]. Higher metastatic ability in 253JB5 cells was associated with higher cytoskeletal fluidity (Fig. 7c). If cytoskeletal fluidity determines the ability of the cell to change shape and contract during motile processes [47], then a shift in cytoskeletal fluidity towards a more fluid-like state may facilitate the shape changes and deformative processes required for invasion of basal lamina, extracellular matrices, and vascular or lymphatic spaces. In that way, changes in cytoskeletal fluidity would emerge as an important mechanism that enables cancer cell dissemination from solid tumors. Data from the human prostate tumor cell lines PC3M and PC3MLN4 cells are consistent with this interpretation. PC3M cells adapted to culture from PC-3 human prostate carcinoma cells are already tumorigenic and metastatic [37]. Repeated cycles of implantation of PC3M cells in the prostate and their extraction from sentinel lymph nodes produced PC3MLN4 cells which show a slightly higher propensity for initiating of distant metastases [37]. Concomitant with an increase in metastatic potential in PC3MLN4 cells was an increase in cytoskeletal fluidity (Fig. 7c). Thus, increased cytoskeletal fluidity may facilitate the basic processes that underlying tissue invasion and vascular access to enable dissemination of primary tumor cells. By a very different mechanism, cytoskeletal fluidity may contribute to the incidence of pulmonary metastasis. The human melanoma cell line A375P is highly tumorigenic but only weakly metastatic [38]. When introduced directly into the peripheral venous circulation, A375P cells are carried to the lung where they may initiate pulmonary metastases [38]. A375P cells are weakly metastatic because large quantities of cells are introduced to produce few lung tumor nodules. A375SM cells were derived from the pulmonary metastases of A375P cells [38]. In contrast to A375P cells, A375SM cells introduced into the circulation produce hundreds of lung tumor nodules in nearly every animal. Similarly, primary renal tumor cells SN12C are highly tumorigenic but weakly metastatic [40]. SN12C cells implanted in the renal parenchyma will develop a primary tumor will eventually gain vascular access but the number of peripheral metastases is typically low. SN12PM6 cells were derived from a single pulmonary metastasis initiated by SN12C cells [41]. SN12PM6 cells produced hundreds of pulmonary metastases in every animal inoculated. For both A375P and SN12C cell lines, cells that initiated pulmonary metastases had lower cytoskeletal fluidity than the parental cell lines (Fig. 7c). One possible explanation for this result is that cancer cells with lower cytoskeletal fluidity, and a more solid-like cytoskeleton, are more likely to survive hematological transport and lodge in the pulmonary micro-circulation. In this view, scores of weakly metastatic cells enter the circulation either directly (A375P cells) or following primary tumor development (SN12C cells). Surviving vascular access and hematological transport requires the cells withstand the fluid forces of the flowing blood. A fluid-like cytoskeleton may be unable to develop the required internal stresses to counteract hematological forces, and they will continually deform to the point of cell destruction by fragmentation [19, 29]. In contrast, a solid-like cytoskeleton may be better able to develop and maintain the internal stresses that are

required to resist lethal deformation, thus, making cells with lower cytoskeletal fluidity more likely to reach the lung. Accommodating the smallest pulmonary capillaries requires the cancer cell to deform and elongate [58], a process that is determined by cellular biophysical properties [59]. A fluid-like cytoskeleton may be better able to deform and flow under hematological forces to accommodate narrow pulmonary capillaries and be transported across the lung. In contrast, a solid-like cytoskeleton may be unable to accommodate narrow pulmonary capillaries, thereby be more likely to lodge within the pulmonary microcirculation and initiate a metastatic lesion. Thus, biophysical assessment of cancer cells in vitro together with their known metastatic phenotypes in vivo suggest that cytoskeletal fluidity seems to capture essential aspects of the physical process of metastasis, thereby providing evidence that biophysical adaptations are a determinant of metastatic ability.

The current approach to investigate the biophysical basis of metastatic ability relied on several important underlying assumptions. The first assumed that the adaptations that induce or enhance metastatic ability also induce biophysical changes in the cell lines tested here. That is, the biophysical adaptations that distinguish strongly and weakly (or non-) metastatic cells emerge out of selection procedures that mimic disease progression in the cancer patient. The extent to which these model systems mimic the biophysical adaptations that may enable cancer progression will remain difficult to assess without knowledge of cancer cell biophysical properties in vivo. However, the cell lines examined here are extremely well-characterized and known to capture the major aspects of cancer progression from primary tumor development to metastatic colonization, thereby proving invaluable in studies of the metastatic process. Importantly, the adaptations that enhance metastatic ability in vivo are preserved through expansion and growth in culture [36–38, 40, 41] making these cell lines extremely useful in investigations of cancer progression in vitro. Nevertheless, relating these new insights derived from biophysical characterization of cultured cells back to metastatic processes that occur in vivo remain at the level of speculation.

The second assumption underlying our approach asserts that OMTC is sensitive to the biophysical changes that enable metastasis. The main determinant of cellular biophysics is the cytoskeleton [60]. Accessing cytoskeletal mechanics through the specific interaction of probe beads to integrin receptors is a strength of the OMTC technique. However, integrin engagement induces pleiotropic signaling events that affect cancer cell biology and mechanics [61, 62]. Furthermore, dysregulation of integrin signaling is coupled to metastatic progression in many cancers [11]. Thus, it is unclear the extent to which the current measurements reflect inherent adaptations in cancer cell biophysics or differences in integrin signaling in cells at different states of cancer progression. Also, cancer cells are typically adherent during metastasis from solid tumors, and a strength of the current experimental approach was the ability to probe cancer cells while adherent to a substrate. While substrate adherence brings important aspects of the metastatic process into the experimental design, adhesion to the uncoated glass surfaces that were used here may confound assessment of cancer cell biophysics. Differences in deformability of adherent human chondrosarcoma cell lines probed by atomic force microscopy diminished or disappeared with incubation time as cell morphology changed from round to spread [63]. Similarly, no difference in deformability was measured between metastatic and nonmetastatic human pancreatic adenocarcinoma cells that were probed by atomic force microscopy while spread [64]. Interestingly, differences in deformability of normal and cancerous human osteoblasts probed by atomic force microscopy were negligible on uncoated glass surfaces but significant on collagen-I coated glass substrates [65]. Thus, while there is some merit to a minimalist experimental approach, it is important to realize that some biophysical adaptations may have become inaccessible leading to the small differences in deformability between cancer cells (Figs. 4a, 5b). It is noteworthy that the induced bead motion used to

probe cancer cells was a small amplitude oscillation imposed around an unstressed state (i.e., no initial force or torque was applied to the beads). During metastasis, cells undergo large deformation while subjected to external forces, e.g., while squeezing across basal lamina into the flowing blood. Thus, biophysical differences between strongly and weakly metastatic cancer cells may emerge only under large forces and deformations. Metastatic and non-metastatic breast cancer cells subjected to a small oscillatory deformation superimposed over an initial stretch using piezoresistive microcantilevers showed differences in deformability that were dependent magnitude of the initially stretch [66]. At low initial stretch, metastatic cells were more deformable than nonmetastatic cells at low frequencies. At higher initial stretch, the opposite behavior emerged: nonmetastatic cells were more deformable than metastatic but only at high frequencies. Thus, key biophysical differences may emerge only at deformations well beyond those imposed with the protocol used here.

Previous efforts to relate metastatic ability to cancer cell biophysics focused almost exclusively on measures of deformability [28, 54, 63, 66–70]. Early approaches combined animal models of cancer development with in vitro biophysical assessment to investigate the role of cancer cell deformability on cancer progression. The elapsed time preceding appearance in the blood following intraperitoneal implantation and number of pulmonary metastases following venous injection of rat ascites hepatoma cells decreased with cell surface deformability assessed by micropipette aspiration [69, 70]. While this approach focused on processes exclusive of tumor formation, these studies showed that vascular access and pulmonary infiltration correlate with cell surface deformability. Interestingly, the pulmonary involvement may depend on the ability of the cells to survive a single passage through a small capillary [69] suggesting that a property of the cell that remains largely unexplored, namely, mechanical integrity, may also contribute to metastatic ability. To include the processes driving escape from solid tumors, mouse B16 melanoma cells were implanted subcutaneously or intramuscularly, developed into primary tumors, and spread to distant organs [28]. Cellular biophysics was assessed by measuring the number of cells traversing a filter under constant pressure, a quantity that depends on a number of biophysical quantities including deformability, integrity, and adhesivity. Nevertheless, cells with a higher propensity to induce distant metastases more easily passed through the filter showing that cancer cell deformability may also contribute to dissemination from solid tumors. Interestingly, when two highly tumorigenic rat fibroblastic cell lines with nearly identical physical properties and ability to colonize the lung were grown into primary tumors, only one was effective in initiating distant metastases [71]. Thus, deformability alone was not sufficient to induce distant metastases from primary tumors. Subsequent studies eschewed the use of animal models to instead assess metastatic ability of human tumor cell lines whose metastatic potential was inferred from their tissue of origin. In a well-characterized model system, non-metastatic MCF-7 breast ductal carcinoma cells were more deformable than normal MCF10A breast mammary epithelial cells whether suspended [67, 68, 72] or adherent [64, 66, 73, 74] with the exception of one study reporting the opposite finding [75]. Further, chemically or genetically increased invasive ability further increased deformability [67, 68, 72, 73]. Similarly, chemically suppressed invasive ability reduced deformability in MDA-MB-231 breast cancer cells [67]. Thus, breast cancer invasive ability is tightly coupled to deformability. As a model system, it is important to note that MCF10 and MCF7 cell lines were derived from independent sources. Thus, there may be inherent differences in their biophysical properties having nothing to do with metastatic ability. In another model system featuring cell lines derived from independent sources, three chondrosarcoma cell lines probed by atomic force microscopy showed that deformability increased, decreased, or not change with increasing metastatic potential [63]. Further, in pancreatic cancer cells derived from the same liver metastasis [76], deformability of metastatic and non-metastatic cells were indistinguishable [64]. The ideal situation would be

to compare cancerous cells at various stages of progression from a single source. Recent developments have allowed deformability to be assessed in cancer cells freshly isolated from cancer patient biopsies [54, 56, 77]. Pleural effusions from patients with suspected lung, breast, and pancreatic cancer yielded cancer cells that were about three times more deformable than normal cells from the same patient [56, 77]. Similarly, primary oral epithelial cells were about three times more deformable than primary oral epithelial cells from healthy volunteers [54]. Interestingly, oral epithelial cancer cells were more deformable from patients whose diagnosis included lymph node involvement than from a single patient whose diagnosis did not include lymph node involvement. The latter finding is important because it shows that biophysical assessment of primary tumor cells may go beyond simply distinguishing cancer cells from normal cells to address a major shortcoming in cancer diagnosis in the clinical setting. Grading of many cancers, including those of the prostate [78], are ineffective at distinguishing low-grade cancers unlikely to impact quality of life from high-grade lesions likely to rapidly progress. Biophysical assessment of cancer cell deformability, or, as suggested by this study, cytoskeletal fluidity, may provide an unbiased quantitative measure of metastatic potential that would provide a key metric to aid in the diagnosis and treatment of many cancers.

When probed by OMTC, transformation by expression of H-ras oncogene in NIH3T3 fibroblast cells or co-over-expression of ErbB2 and 14-3-3-ζ in MCF10A cells increased stiffness relative to control cell lines. Transformation typically decreases cell stiffness [24, 25, 54, 56, 60, 67, 68, 71, 79–85]. Transformation is associated with a reduction in cell adhesivity and spreading [25]. Cell morphology is closely associated to cytoskeletal deformability, with well-spread cells stiffer than round cells [86] presumably because of higher cytoskeletal forces in distended cells [87]. In MCF10A cells, transformation by ErbB2 and 14-3-3-ζ overexpression lead to increased cell spreading: MCF10A-V cells exhibit a rounded cobblestone-like epithelial morphology whereas MCF10A-ErbB2-ζ assume a more spindle-like morphology with many cells surrounded by broad, thin lamellipodia [33]. The increase in cell spreading in MCF10A-ErbB2-ζ cells was associated with higher stiffness (Figs. 4b, 5b). Transformation by overexpression of ErbB2 and 14-3-3-ζ seemed to increase cell stiffness by inducing cell spreading. Partial transformation by overexpression of ErbB2 alone supports this interpretation, but overexpression of 14-3-3-ζ alone does not. MCF10A-ErbB2 cells that maintain the same cobblestone-like epithelial morphology as MCF10A-V cells [33] and have the similar stiffness (Figs. 4b, 5b). MCF10A-ζ cells are spindle-like with even more prominent surrounding lamellipodia than MCF10A-ErbB2-ζ cells [33], yet, MCF10A-ζ cells have the lowest stiffness (Figs. 4b, 5b). Interestingly, under very different conditions, deformability of all three oncoprotein overexpressing cells followed the same qualitative trends as was measured by OMTC (Fig. 5b): MCF10A-ErbB2 and MCF10A-ErbB2-ζ cells were less deformable and MCF10A-ζ cells more deformable than MCF10A-V cells [73]. Thus, overexpression of ErbB2 and 14-3-3-ζ appears to induce transformation without the expected biophysical consequences of cell rounding and cytoskeletal softening. Transformed fibroblasts, however, were more deformable than normal fibroblasts when probed by cell poking, micropipette aspiration, atomic force microscopy, and optical stretching [24, 25, 60, 67, 71, 82, 84]. One difference between the current approach and all previous approaches is in probe specificity. Previous methods probe the cells nonspecifically, thereby measuring primarily bulk cellular properties. In this investigation, cells were probed across specific molecular pathways linking surface adhesion receptors to intracellular cytoskeletal filaments. Specifically, binding RGD-coated beads to cell surface receptors induces local cytoskeletal reorganization, thereby influencing cytoskeletal biophysics [49]. It is possible that the twofold increase in cellular deformability measured in transformed cells by other techniques is overwhelmed by local cytoskeletal remodeling in the vicinity of the probe in OMTC measurements. A better approach to distinguish normal and transformed cells by OMTC

might be to use beads coated with ligands that bind integrin receptors without activation [49] or bind other surface receptors without inducing cytoskeletal alterations [53].

Histograms of the logarithm of g', the logarithm of g'', and x measured in all cell lines appeared normally distributed (Figs. 5, 6,7a) in agreement with previous results [44, 88]. Differences in mean values between strongly and weakly metastatic cell lines were often small (Figs. 5b, 6b, 7c). Collecting large samples (Table 1) allows these distributions to be determined with high accuracy. Thus, even small differences in mean values are real and resolved with statistical significance (Figs. 5, 6c). In the case of cytoskeletal fluidity, deviations from normality emerge at high x (Fig. 7b). Mean values of x between strongly and weakly metastatic cells were compared using the two-sample z procedure (z test) which requires only that the samples be independent and large (sample size = 30), but not normal, and the non-pooled t-procedure (t test) which assumes normally distributed data [50]. Two-tailed z and t tests evaluated at 5 % probability produced identical outcomes: the differences in x between strongly and weakly metastatic cell lines were significant (Fig. 7b). More importantly, however, differences in g', g'', and x were systematic, repeatable, and physiologically important. For example, even modest 5 % increases in fluidity produce 10 % increases in fluidization in response to stretch [89], twofold increases in cytoskeletal friction [15] and rate of cytoskeletal remodeling [16], and threefold reductions in cytoskeletal stiffness [15]. As such, the associated functional consequences of small changes in x are profound.

The phenomenological parameter x is a direct measure of cytoskeletal fluidity (Eq. 2). It has its origins in a novel integrative framework of cytoskeletal biophysics and brings together into one physical picture the most basic biophysical properties of the cytoskeleton: elastic energy storage, mechanical energy dissipation, and structural remodeling [47, 48, 90, 91]. Since these basic processes determine the ability of the cell to deform, flow, remodel, and contract, they inherently underlie higher cellular functions key to metastatic dissemination of primary tumor cells, namely shape change, force generation, and cellular motility. Thus, cytoskeletal fluidity as a primary determinant of metastatic potential could unify our understanding of the basic biophysical processes driving metastatic dissemination of primary tumor cells. Perhaps more importantly, measurements of cytoskeletal fluidity in the clinical setting could provide a quantitative index of metastatic potential to aid in diagnosis and treatment of cancer patients.

Metastasis is fundamentally a mechanical process, yet, the biophysical contributions to metastatic ability remain largely unidentified. We found that metastatic ability correlates with a novel biophysical parameter, the cytoskeletal fluidity. As such measurements of cytoskeletal fluidity both in the laboratory and in the clinic could provide a quantitative and unbiased snapshot of metastatic ability that may prove instrumental in advancing our understanding of cancer progression.

Acknowledgments

Transfected MCF-10A cell lines were a kind gift from Dr. Muhammad Zaman (Boston University, Boston, MA).The cancer cell lines 253J, 253JB5, A375P, A375SM, PC3M, PC3MLN4, SN12C, and SN12PM6 were kindly provided by Dr. Isaiah J. Fidler (M.D. Anderson Cancer Center, Houston, TX). G.L. was supported by the Parker B. Francis Foundation. D.R.B. was funded by NCI CA118732 and CA155728. J.J.F. was funded by R01HL107561, R01HL102373, and R01EY019696.

References

1. Sporn MB. The war on cancer. Lancet. 1996; 347:1377–1381. [PubMed: 8637346]

2. Chambers AF, Groom AC, MacDonald IC. Dissemination and growth of cancer cells in metastatic sites. Nat Rev Cancer. 2002; 2:563–572. [PubMed: 12154349]
3. Gupta GP, Massagué J. Cancer metastasis: building a framework. Cell. 2006; 127:679–695. [PubMed: 17110329]
4. Hanahan D, Weinberg RA. The hallmarks of cancer. Cell. 2000; 100:57–70. [PubMed: 10647931]
5. Perou CM, Sørlie T, Eisen MB, Rijn Mvd, Jeffrey SS, Rees CA, Pollack JR, Ross DT, Johnsen H, Akslen LA, Fluge Ø , Pergamenschikov A, Williams C, Zhu SX, Lønning PE, Børresen-Dale A-L, Brown PO, Botstein D. Molecular portraits of human breast tumors. Nature. 2000; 406:747–752. [PubMed: 10963602]
6. Futreal PA, Coin L, Marshall M, Down T, Hubbard T, Wooster R, Rhaman N, Stratton MR. A census of human cancer genes. Nat Rev Cancer. 2004; 4:177–183. [PubMed: 14993899]
7. Coussens LM, Werb Z. Matrix metalloproteinases and the development of cancer. Chem Biol. 1996; 3(11):895–904. [PubMed: 8939708]
8. Coussens LM, Fingleton B, Matrisan LM. Matrix metalloproteinase inhibitors and cancer: trials and tribulations. Science. 2002; 295:2387–2992. [PubMed: 11923519]
9. Egeblad M, Werb Z. New functions for the matrix metalloproteinases in cancer progression. Nat Rev Cancer. 2002; 2:161–174. [PubMed: 11990853]
10. Cavallaro U, Christofori G. Cell adhesion and signaling by cadherins and Ig-CAMs in cancer. Nat Rev Cancer. 2004; 4:118–132. [PubMed: 14964308]
11. Guo W, Giancotti FG. Integrin signaling during tumor progression. Nat Rev Cancer. 2004; 5:816–826.
12. Raz A, Geiger B. Altered organization of cell-substrate contacts and membrane-associated cytoskeleton in tumor cell variants exhibiting different metastatic capabilities. Cancer Res. 1982; 42:5183–5190. [PubMed: 7139623]
13. Paszek MJ, Zahir N, Johnson KR, Lakins JN, Rozenberg GI, Gefen A, Reinhart-King CA, Margulies SS, Dembo M, Boettiger D, Hammer DA, Weaver VM. Tensional homeostasis and the malignant phenotype. Cancer Cell. 2005; 8(3):241–254. [PubMed: 16169468]
14. Stamenovic D, Fredberg JJ, Wang N, Butler JP, Ingber DE. A microstructural approach to cytoskeletal mechanics based on tensegrity. J Theor Biol. 1996; 181:125–136. [PubMed: 8935591]
15. Fabry B, Maksym GN, Butler JP, Glogauer M, Navajas D, Fredberg JJ. Scaling the microrheology of living cells. Phys Rev Lett. 2001; 87(14):148102. [PubMed: 11580676]
16. Bursac P, Lenormand G, Fabry B, Oliver M, Weitz DA, Viasnoff V, Butler JP, Fredberg JJ. Cytoskeletal remodeling and slow dynamics in the living cell. Nat Mater. 2005; 4:557–561. [PubMed: 15937489]
17. Wang N, Tolic-Nørrelykke IM, Chen J, Mijailovich SM, Butler JP, Fredberg JJ, Stamenovic D. Cell prestress I. Stiffness and prestress are closely associated in adherent contractile cells. Am J Physiol Cell Physiol. 2002; 282(3):C606–C616. [PubMed: 11832346]
18. Laudadio RE, Millet EJ, Fabry B, An SS, Butler JP, Fredberg JJ. Rat airway smooth muscle cell during actin modulation: rheology and glassy dynamics. Am J Physiol Cell Physiol. 2005; 298(6):C1388–C1395. [PubMed: 16120653]
19. Wyckoff JB, Jones JG, Condeelis JS, Segall JE. A critical step in metastasis: in vivo analysis of intravasation at the primary tumor. Cancer Res. 2000; 60(9):2504–2511. [PubMed: 10811132]
20. Shestakova EA, Wyckoff J, Jones J, Singer RH, Condeelis J. Correlation of beta-actin messenger RNA localization with metastatic potential in rat adenocarcinoma cell lines. Cancer Res. 1999; 59:1202–1205. [PubMed: 10096548]
21. Soon L, Braet F, Condeelis J. Moving in the right direction-nanoimaging in cancer cell motility and metastasis. Microsc Res Tech. 2007; 70:252–257. [PubMed: 17279509]
22. Sahai E, Marshall CJ. RHO-GTPases and cancer. Nat Rev Cancer. 2002; 2:133–142. [PubMed: 12635176]
23. Yamazaki D, Kurisu S, Takenawa T. Regulation of cancer cell motility through actin reorganization. Cancer Sci. 2005; 96(7):379–386. [PubMed: 16053508]
24. Erickson CA. The deformability of BHK cells and polyoma virus-transformed BHK cells in relation to locomotory behavior. J Cell Sci. 1980; 44:187–200. [PubMed: 6254999]

25. Thoumine O, Ott A. Comparison of the mechanical properties of normal and transformed fibroblasts. Biorheology. 1997; 34(4/5):309–326. [PubMed: 9578806]
26. Brooks DE. The biorheology of tumor cells. Biorheology. 1984; 21:85–91. [PubMed: 6466799]
27. Weiss L, Asch BB, Elkin G. Effects of cytoskeletal perturbation on the sensitivity of ehrlich ascites tumor cell surface membranes to mechanical trauma. INV Met. 1991; 11:93–101.
28. Ochalek T, Nordt FJ, Tullberg K, Burger MM. Correlation between cell deformability and metastatic potential in B16-F1 melanoma cell variants. Cancer Res. 1988; 48:5124–5128. [PubMed: 3409238]
29. Wang W, Wyckoff JB, Frohlich VC, Oleynikov Y, Hüttelmaier S, Zavadil J, Cermak L, Bottinger EP, Singer RH, White JG, Segall JE, Condeelis JS. Single cell behavior in metastatic primary mammary tumors correlated with gene expression patterns revealed by molecular profiling. Cancer Res. 2002; 62(21):6278–6288. [PubMed: 12414658]
30. Egan SE, McClarty GA, Jarolm L, Wright JA, Spiro I, Hager G, Greenberg AH. Expression of H-ras correlates with metastatic potential: evidence for regulation of the metastatic phenotype in 10T1/2 and NIH 3T3 cells. Mol Cell Biol. 1987; 7(2):830–837. [PubMed: 3102946]
31. Soule HD, Maloney TM, Wolman SR, Ward J, Peterson D, Brenz R, McGrath CM, Russo J, Pauley RJ, Jones RF, Brooks SC. Isolation and characterization of a spontaneously immortalized human breast epithelial cell line, MCF-10. Cancer Res. 1990; 50:6075–6086. [PubMed: 1975513]
32. Debnath J, Muthuswamy SK, Brugge JS. Morphogenesis and oncogenesis of MCF-10A mammary epithelial acini grown in three-dimensional basement membrane cultures. Methods. 2003; 30:256–268. [PubMed: 12798140]
33. Lu J, Guo H, Treekitkarnmongkol W, Li P, Zhang J, Shi B, Ling C, Zhou X, Chen T, Chiao PJ, Feng X, Seewaldt VL, Muller WJ, Sahin A, Hung M- C, Yu D. 14-3-3-f cooperates with ErbB2 to promote ductal carcinoma in situ progression to invasive breast cancer by inducing epithelial–mesenchymal transition. Cancer Cell. 2009; 16:195–207. [PubMed: 19732720]
34. Tambe DT, Hardin CC, Angelini TE, Rajendran K, Park CY, Serra-Picamal X, Zhou EH, Zaman MH, Butler JP, Weitz DA, Fredberg JJ, Trepat X. Collective cell guidance by cooperative intercellular forces. Nat Mater. 2011; 10:469–475. [PubMed: 21602808]
35. Elliott AY, Cleveland P, Cervenka J, Castro AE, Stein N, Hakala TR, Fraley EE. Characterization of a cell line from human transitional cell cancer of the urinary tract. J Nat Cancer Inst. 1974; 53(5):1341–1349. [PubMed: 4431054]
36. Dinney CPN, Fishbeck R, Singh RK, Eve B, Pathak S, Brown N, Xie B, Fan D, Bucana CD, Fidler IJ, Killion JJ. Isolation and characterization of metastatic variants from human transitional cell carcinoma passaged by orthotropic implantation in athymic nude mice. J Urol. 1995; 154:1532–1538. [PubMed: 7658585]
37. Pettaway CA, Pathak S, Greene G, Ramirez E, Wilson MR, Killion JJ, Fidler IJ. Selection of highly metastatic variants of different human prostatic carcinomas using orthotropic implantation in nude mice. Clin Cancer Res. 1996; 2:1627–1636. [PubMed: 9816342]
38. Kozlowski JM, Fidler IJ, Campbell D, Xu Z-l, Kaighn ME, Hart IR. Metastatic behavior of human tumor cell lines grown in the nude mouse. Cancer Res. 1984; 44:3522–3529. [PubMed: 6744277]
39. Kozlowski JM, Hart IR, Fidler IJ, Hanna N. A human melanoma line heterogeneous with respect to metastatic capacity in athymic nude mice. J Nat Cancer Inst. 1984; 72:913–917. [PubMed: 6584666]
40. Naito S, Eschenbach AC v, Giavazzi R, Fidler IJ. Growth and metastasis of tumor cells isolated from a human renal cell carcinoma implanted into different organs of nude mice. Cancer Res. 1986; 46:4109–4115. [PubMed: 3731078]
41. Naito S, Walker SM, Fidler IJ. In vivo selection of human renal cell carcinoma cells with high metastatic potential in nude mice. Clin Exp Metastasis. 1989; 7(4):381–389. [PubMed: 2706827]
42. Fabry B, Maksym GN, Shore SA, Moore PE, Reynold J, Panettieri A, Butler JP, Fredberg JJ. Time course and heterogeneity of contractile responses in cultured human airway smooth muscle cells. J Appl Physiol. 2001; 91:986–994. [PubMed: 11457818]
43. Wang N, Butler JP, Ingber DE. Mechanotransduction across the cell surface and through the cytoskeleton. Science. 1993; 260:1124–1127. [PubMed: 7684161]

44. Fabry B, Maksym GN, Butler JP, Glogauer M, Navajas D, Ta-back NA, Millet EJ, Fredberg JJ. Time scale and other invariants of integrative mechanical behavior in living cells. Phys Rev E. 2003; 68(041914):041914.
45. Puig-de-Morales-Marinkovic M, Turner KT, Butler JP, Fredberg JJ, Suresh S. Viscoelasticity of the human red blood cell. Am J Cell Physiol. 2007; 293:C597–C605.
46. Valberg PA, Butler JP. Magnetic particle motions within living cells. Physical theory and techniques. Biophys J. 1987; 52:537–550. [PubMed: 3676435]
47. Lenormand G, Fredberg JJ. Deformability, dynamics, and remodeling of cytoskeleton of the adherent living cell. Biorheology. 2006; 43(1):1–30. [PubMed: 16627924]
48. Sollich P. Rheological constitutive equation for a model of soft glassy materials. Phys Rev E. 1998; 58(1):738–759.
49. Puig-de-Morales M, Millet E, Fabry B, Navajas D, Wang N, Butler JP, Fredberg JJ. Cytoskeletal mechanics in the adherent human airway smooth muscle cells: probe specificity and scaling of protein–protein dynamics. Am J Physiol Cell Physiol. 2004; 287(3):C643–C654. [PubMed: 15175221]
50. Weiss, NA.; Hassett, MJ. Introductory statistics. Addison-Wesley; Reading: 1991.
51. Lenormand G, Millet E, Fabry B, Butler JP, Fredberg JJ. Linearity and time-scale invariance of the creep function in living cells. J R Soc Interface. 2004; 1(1):91–97. [PubMed: 16849155]
52. Fielding SM, Sollich P, Cates ME. Aging and rheology in soft materials. J Rheol. 2000; 44(2): 323–369.
53. Coughlin MF, Puig-de-Morlaes M, Bursac P, Mellema M, Millet E, Fredberg JJ. Filamin-A and rheological properties of cultured melanoma cells. Biophys J. 2006; 90(6):2199–2205. [PubMed: 16387775]
54. Remmerbach TW, Wottawah F, Dietrich J, Lincoln B, Wittekind C, Guck J. Oral cancer diagnosis by mechanical pheno-typing. Cancer Res. 2009; 69(5):1728–1732. [PubMed: 19223529]
55. Darling EM, Topel M, Zauscher S, Vail TP, Guilak F. Viscoelastic properties of human mesenchymally-derived stem cells and primary osteoblasts, chondrocytes, and adipocytes. J Biomech. 2008; 41:454–464. [PubMed: 17825308]
56. Cross SE, Jin Y, Rao J, Gimzewski JK. Nanomechanical analysis of cells from cancer patients. Nat Nanotechnol. 2007; 2:780–783. [PubMed: 18654431]
57. Rosenbluth MJ, Lam WA, Fletcher DA. Force microscopy of nonadherent cells: a comparison of leukemia cell deformability. Biophys J. 2006; 90:2994–3003. [PubMed: 16443660]
58. Weiss L. Biomechanical interactions of cancer cells with the microvasculature during hematogenous metastasis. Cancer Metastasis Rev. 1992; 11:227–235. [PubMed: 1423815]
59. Worthen GS, Schwab B III, Elson EL, Downey GP. Mechanics of stimulated neutrophils: cell stiffening induces retention in capillaries. Science. 1989; 245:183–186. [PubMed: 2749255]
60. Petersen NO, McConnaughey WB, Elson EL. Investigations of structural determinants of cell shape. Commun Mol Cell Biophys. 1981; 1(3):135–147.
61. Desgrosellier JS, Cheresh DA. Integrins in cancer: biological implications and therapeutic opportunities. Nat Rev Cancer. 2010; 10:9–22. [PubMed: 20029421]
62. Varner JA, Cheresh DA. Integrins and cancer. Curr Opin Cell Biol. 1996; 8:724–730. [PubMed: 8939661]
63. Darling EM, Zauscher S, Block JA, Guilak F. A thin-layer model for viscoelastic, stress-relaxation testing of cells using atomic force microscopy: do cell properties reflect metastatic potential? Biophys J. 2007; 92:1784–1791. [PubMed: 17158567]
64. Li Y, Schnekenburger J, Duits MGH. Intracellular particle tracking as a tool for tumor cell characterization. J Biomed Opt. 2009; 14(6):064005. [PubMed: 20059243]
65. Docheva D, Padula D, Popov C, Mutschler W, Clausen-Schaumann H, Schieker M. Researching into the cellular shape, volume and elasticity of mesenchymal stem cells, osteoblasts and osteosarcoma cells by atomic force microscopy. J Cell Mol Med. 2008; 12(2):537–552. [PubMed: 18419596]

66. Shim S, Kim MG, Jo K, Kang YS, Lee B, Yang S, Shin S- M, Lee J- H. Dynamic characterization of human breast cancer cells using a piezoresistive microcantilever. J Biomech Eng. 2010; 132:104501. [PubMed: 20887019]

67. Guck J, Schinkinger S, Lincoln B, Wottawah F, Ebert S, Romeyke M, Lenz D, Erickson HM, Ananthakrishnan R, Mitchell D, Käs J, Ulvick S, Bilby C. Optical deformability as an inherent cell marker for testing malignant transformation and metastatic competence. Biophys J. 2005; 88(5): 3689–3698. [PubMed: 15722433]

68. Lincoln B, Erickson HM, Schinkinger S, Wottawah F, Mitchell D, Ulvick S, Bilby C, Guck J. Deformability-based flow cytometry. Cytometry A. 2004; 59A:203–209. [PubMed: 15170599]

69. Sato, H.; Suzuki, M. Deformability and viability of tumor cells by transcapillary passage, with reference to organ affinity of metastasis in cancer.. In: Weiss, L., editor. Functional aspects of metastasis. North-Holland; Amsterdam: 1976. p. 311-317.

70. Sato H, Khato J, Sato T, Suzuki M. Deformability and filterability of tumor cells through “Nucleopore” filter, with reference to viability and metastatic spread. GANN Monogr Cancer Res. 1977; 20:3–13.

71. Ward KA, Li W- I, Zimmer S, Davis T. Viscoelastic properties of transformed cells: role in tumor cell progression and metastasis formation. Biorheology. 1991; 28(3–4):301–313. [PubMed: 1932719]

72. Bao N, Zhan Y, Lu C. Microfluidic electroporative flow cytometry for studying single-cell biomechanics. Anal Chem. 2008; 80:7714–7719. [PubMed: 18798650]

73. Baker EL, Lu J, Yu D, Bonnecaze RT, Zaman MH. Cancer cell stiffness: integrated roles of three-dimensional matrix stiffness and transforming potential. Biophys J. 2010; 99:2048–2057. [PubMed: 20923638]

74. Li QS, Lee GYH, Ong CN, Lim CT. AFM indentation study of breast cancer cells. Biochem Biophys Res Commun. 2008; 374:609–613. [PubMed: 18656442]

75. Guido I, Jaeger MS, Duschl C. Dielectrophoretic stretching of cells allows for characterization of their mechanical properties. Eur Biophys J. 2011; 40:281–288. [PubMed: 21110017]

76. Elsässer H-P, Lehr U, Agricola B, Kern HF. Establishment and characterisation of two cell lines with different grade of differentiation derived from one primary human pancreatic adenocarcinoma. Virchows Arch B Cell Pathol. 1992; 61:295–306.

77. Cross SE, Jin Y- S, Tondre J, Wong R, Rao JY, Gimzewski JK. AFM-based analysis of human metastatic cancer cells. Nanotechnology. 2008; 19:384003. [PubMed: 21832563]

78. Oh, WK.; Hurwitz, M.; D'Amico, AV.; Richie, JP.; Kantoff, PW. Neoplasms of the prostate.. In: Kufe, DW., editor. Cancer medicine. 6th edn.. Decker; Hamilton: 2003. p. 1707-1740.

79. Anderson KW, Li W- I, Cezeaux J, Zimmer S. In vitro studies of deformation and adhesion properties of transformed cells. Cell Biophys. 1992; 18(2):81–97. [PubMed: 1726528]

80. Lekka M, Laidler P, Gil D, Lekki J, Stachura Z, Hrynkiewicz AZ. Elasticity of normal and cancerous human bladder cells studied by scanning force microscopy. Eur Biophys J. 1999; 28:312–316. [PubMed: 10394623]

81. Lekka M, Laidler P, Ignacak J, Labedz M, Lekki J, Struszczyk H, Stachura Z, Hrynkiewicz AZ. The effect of chitosan on stiffness and glycolytic activity of human bladder cells. Biochim Biophys Acta. 2001; 1540:127–136. [PubMed: 11513974]

82. Park S, Koch D, Cardenas R, Käs J, Shih CK. Cell motility and local viscoelasticity of fibroblasts. Biophys J. 2005; 89:4330–4342. [PubMed: 16199496]

83. Reed J, Frank M, Troke JJ, Schmit J, Han S, Teitell MA, Gimzewski JK. High throughput cell nanomechanics with mechanical imaging interferometry. Nanotechnology. 2008; 19:235101. [PubMed: 20737027]

84. Wottawah F, Schinkinger S, Lincoln B, Anathakrishnan R, Romeyke M, Guck J, Käs J. Optical rheology of biological cells. Phys Rev Lett. 2005; 94:098103. [PubMed: 15784006]

85. Zhang G, Long M, Wu Z- Z, Yu W- Q. Mechanical properties of hepatocellular carcinoma cells. World J Gastroenterol. 2002; 8(2):243–246. [PubMed: 11925600]

86. Wang N, Ingber DE. Control of cytoskeletal mechanics by extracellular matrix, cell shape, and mechanical tension. Biophys J. 1994; 66(June):2181–2189. [PubMed: 8075352]

87. Coughlin MF, Stamenovic D. A tensegrity model of the cytoskeleton in spread and round cells. J Biomech Eng. 1998; 120(6):770–777. [PubMed: 10412462]

88. Balland M, Desprat N, Icard D, Féréol S, Asnacios A, Browaeys J, Hénon S, Gallet F. Power laws in microrheology experiments on living cells: comparative analysis and modeling. Phys Rev E. 2006; 74:021911.

89. Trepat X, Deng L, An SS, Navajas D, Tschumperlin DJ, Gerthoffer WT, Butler JP, Fredberg JJ. Universal physical responses to stretch in the livingcell. Nature. 2007; 447:592–596. [PubMed: 17538621]

90. Fabry B, Fredberg JJ. Remodeling of the airway smooth muscle cell: are we built of glass. Respir Physiol Neurobiol. 2003; 137(2–3):109–124. [PubMed: 14516720]

91. Sollich P, Lequeux F, Hébraud P, Cates ME. Rheology of soft glassy materials. Phys Rev Lett. 1997; 78(10):2020–2023.

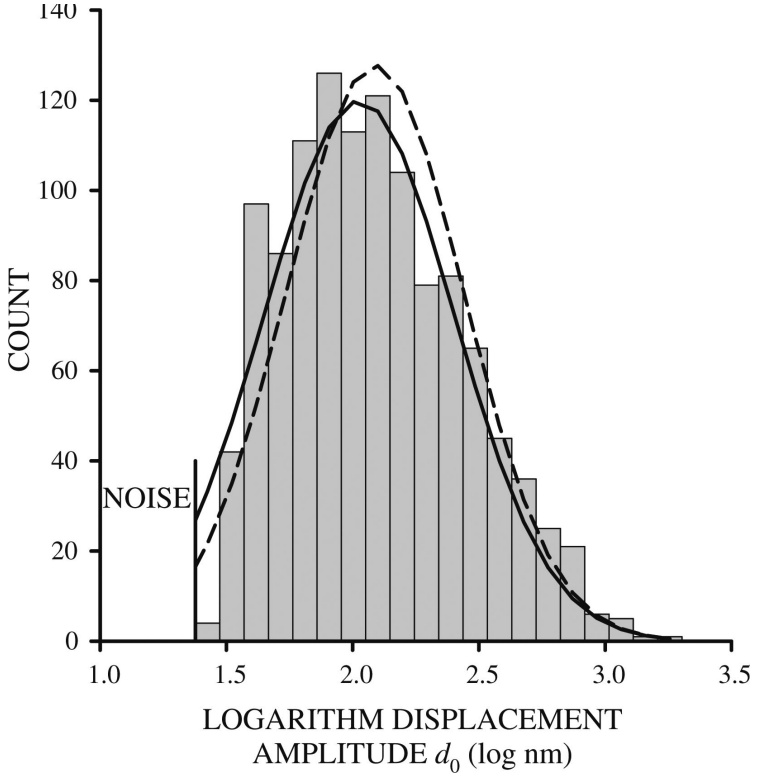

Fig. 1.

Histogram of the logarithm of bead displacement amplitude d_0 for 253J cells at 0.1 Hz. The histogram is truncated at low displacements because beads whose amplitude is below the level of system noise were excluded from analysis. Using the mean and standard deviation computed from the truncated distribution produces normal curves that are shifted to higher displacement values (*dashed line*). Fitting the normal curve to the truncated distribution produced lower error between data and normal curve (*solid line*) measured by the sum of the squared differences at each bin midpoint

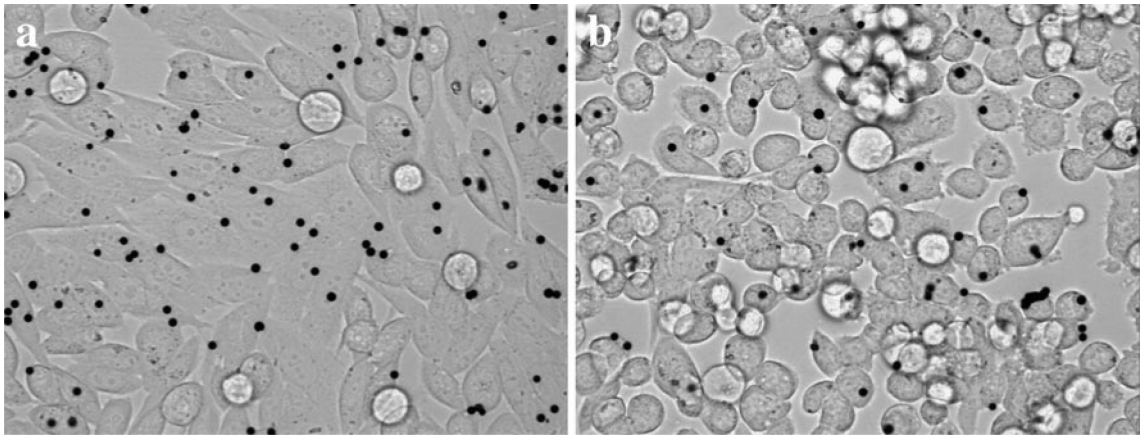

Fig. 2.
Glass-adherent **a** PC3M and **b** PC3MLN4 cells with attached RGD-coated magnetic beads (*black circles*) for OMTC measurements. Beads came into sharp focus above the apical cell surface indicating that the beads were sitting on top of the cells

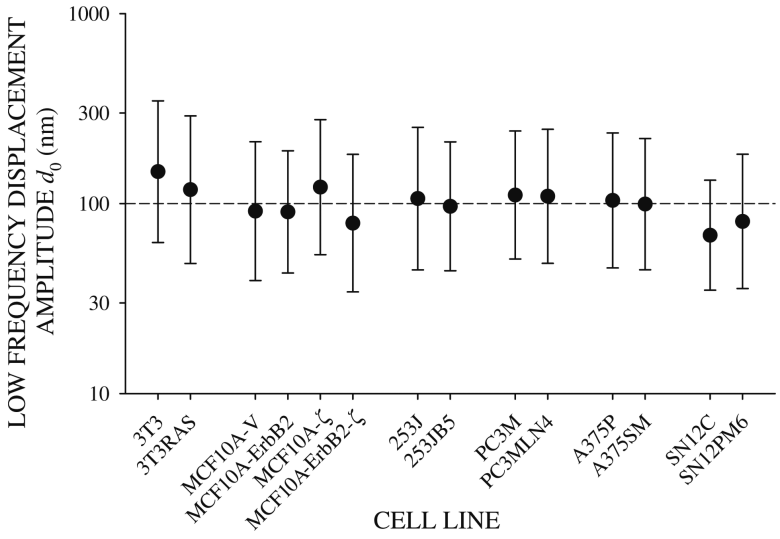

Fig. 3.

Bead displacement amplitude d_0 at the low frequency $f = 0.1$ Hz for all cell lines tested. Mean bead displacement was near 100 nm (*dashed line*)

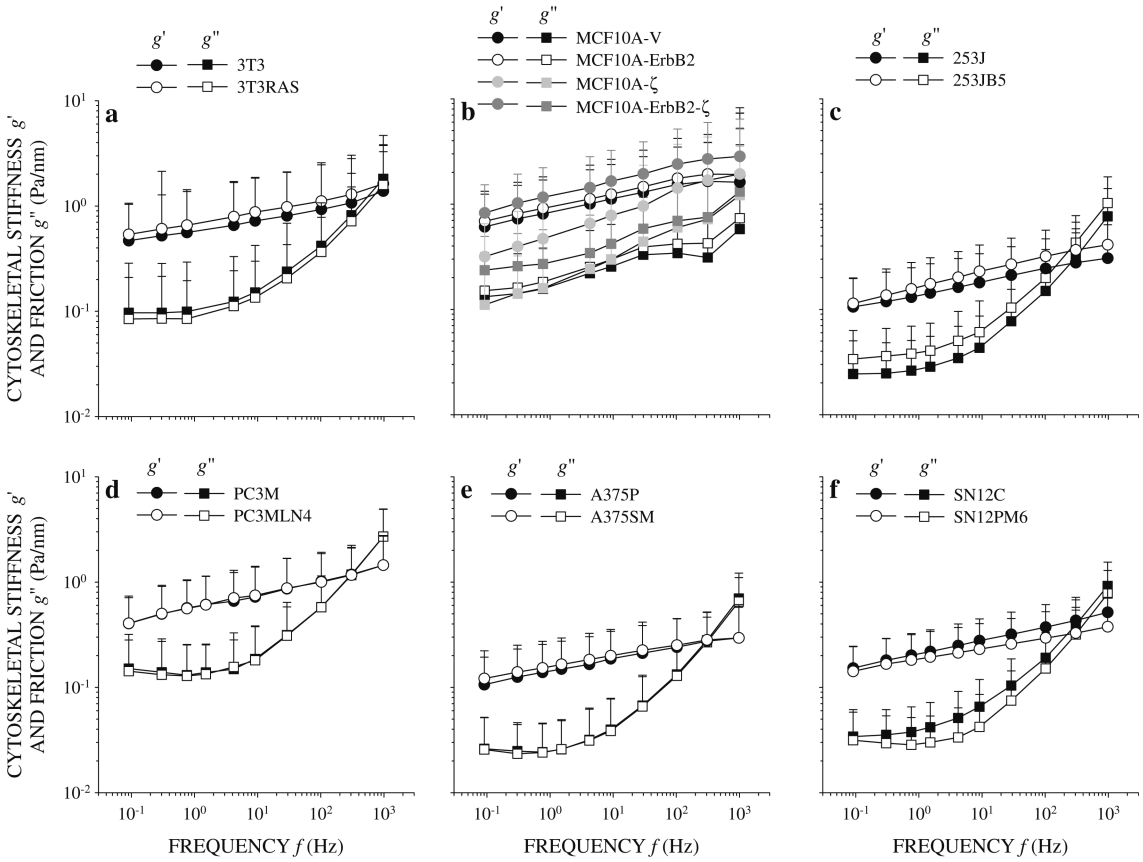

Fig. 4.

Mean and standard deviation of cytoskeletal stiffness g' and friction g'' of **a** 253J (*black symbols*) and 253JB5 (*white symbols*) cells, **b** MCF10-V (*black*), MCF10A-ErbB (*white*), MCF10A-ζ (*light grey*), and MCF10A-ErbB2-ζ (*dark grey*), **c** 253J (*black*) and 253JB5 (*white*) cells, **d** PC3M (*black*) and PC3MLN4 (*white*) cells, **e** A375P (*black*) and A375SM (*white*) cells, **f** SN12C (*black*) and SN12PM6 (*white*) cells. Stiffness increased as a power law of the oscillatory frequency f as seen by the nearly linear dependence of g' on f on log–log scales. Friction g'' at low frequencies increased, remained constant, or decreased with increasing frequency. All cells except the MCF10 group (**b**) exhibited strong frequency dependence at high frequencies consistent with viscous dissipation

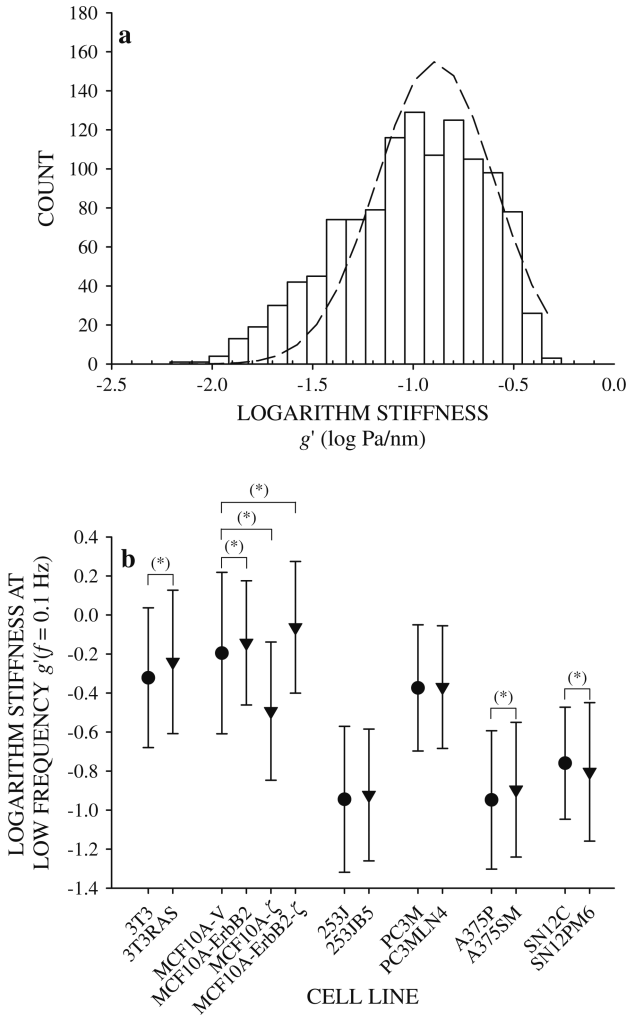

Fig. 5.

Cytoskeletal stiffness g' at the lowest measured frequency $f = 0.1$ Hz for 253J cells was log-normally distributed, thus **a** the logarithm of g' is distributed nearly normally (*dashed line*). Logarithm of g' of all cell lines appeared normally distributed, so mean values of the logarithm of stiffness were compared by *z* test between cells within each group. **b** Comparison of logarithm of stiffness g' at the lowest measured frequency $f = 0.1$ Hz of all cell line groups (mean ± standard deviation). Significant difference in mean values* ($P = 5$ %)

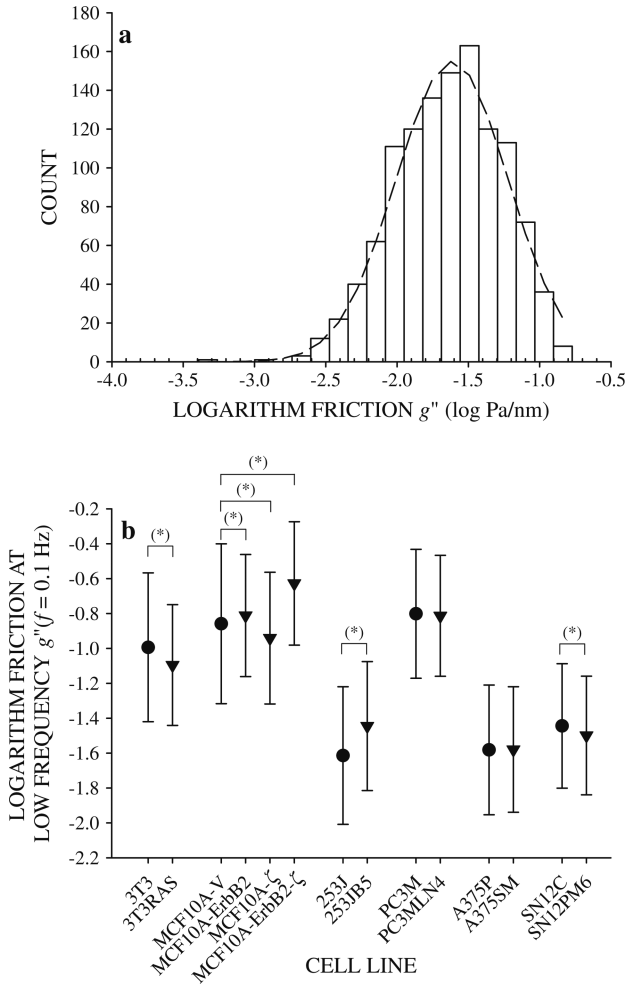

Fig. 6.

Cytoskeletal friction g'' at the lowest measured frequency $f = 0.1$ Hz for 253J cells was log-normally distributed. **a** The logarithm of g'' is distributed nearly normally (*dashed line*). Logarithm of g'' of all cell lines appeared normally distributed, so mean values of the logarithm of friction were compared by *z* test between cells within each group. **b** Comparison of logarithm of friction g'' at the lowest measured frequency $f = 0.1$ Hz for all cell line groups (mean ± standard deviation). Significant difference in mean values* ($P = 5$ %)

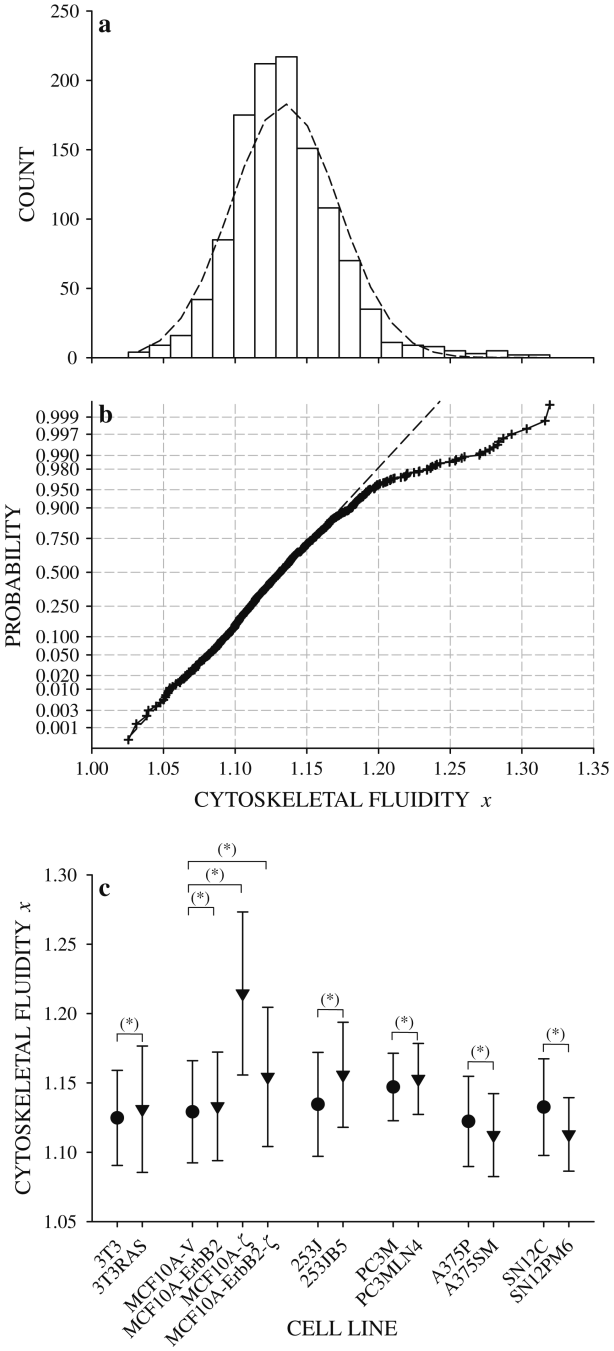

Fig. 7.

a Distribution of cytoskeletal fluidity *x* for 253J cells with superimposed normal curve (*dashed line*). The distribution of *x* for other cell lines was similar. **b** Normal probability plot of cytoskeletal fluidity *x* for 253J cells. Deviations from linearity at high *x* indicate a heavier right tail than would be expected for a normal distribution. *c* Comparison of cytoskeletal fluidity *x* between cell lines within each group by *z* test (mean ± standard deviation). Significant difference in mean values* (*P* = 5 %)

Table 1

For each cell line, the total number of beads tracked by OMTC

Cell Type	Total	Analyzed	Rejected
NIH3T3	822	714 (87 %)	108 (13 %)
RAS NIH3T3	431	302 (70 %)	129 (30 %)
MCF10A-V	1983	1167 (59 %)	816 (51 %)
MCF10A-ErbB2	1821	886 (49 %)	935 (51 %)
MCF10A-ζ	442	270 (61 %)	172 (39 %)
MCF10A-ErbB2-ζ	1340	466 (35 %)	874 (65 %)
A375P	1825	1425 (78 %)	400 (22 %)
A375SM	1773	1452 (82 %)	321 (18 %)
SN12C	2159	1242 (58 %)	917 (42 %)
SN12PM6	2622	1892 (72 %)	730 (28 %)
253J	1423	1169 (82 %)	254 (18 %)
253JB5	1466	1006 (69 %)	460 (31 %)
PC3M	333	266 (80 %)	67 (20 %)
PC3MLN4	400	332 (83 %)	68 (17 %)

The number of beads that were analyzed and found to probe the cell in the linear regime, and the number of beads that were rejected for displaying a nonlinear mechanical response during oscillatory twisting